View metadata, citation and similar papers at core.ac.uk
brought to you by CORE
provided by Institutionelles Repositorium der Leibniz Universität Hannover

Constrained Design of Multisine Signals for Frequency-domain Identification of Electric Drive Trains

Mathias Tantau * **Thomas Petersen** ** **Mark Wielitzka** * **Tobias Ortmaier** *

* *Leibniz University Hanover, Institute of Mechatronic Systems, An der Universität 1, 30823 Garbsen, Germany (e-mail: mathias.tantau@imes.uni-hannover.de)*
** *Lenze Automation GmbH, Am Alten Bahnhof 11, 38122 Braunschweig, Germany*

Abstract: The paper at hand deals with the optimization of multisine signals in terms of effective value for identification of electric drive trains, considering constraints on position, velocity, acceleration and torque. The advantage of maximizing the effective value while respecting the constraints rather than minimizing the crest factor of the input signal is delineated. Results with two algorithms suitable for this optimization task are presented for different sets of dynamic constraints. It is shown that the proposed modified clipping algorithm is much faster than the L_∞ optimization which is dedicated to simultaneous optimization of several different signals, while being slightly less performant in terms of effective value.

Keywords: multisine excitation, optimized multisine, optimal excitation, design of experiment, experimental modal testing, frequency-domain identification.

1. INTRODUCTION

Optimized multisine signals, also called multi-frequency excitation (MFE) signals are commonly used for frequency response function (FRF) measurements because of their short experimental duration in contrast to stepped sines and the possibility to specify the exact spectrum as opposed to pseudo-random binary sequence signals (PRBS), random noise and others (Pintelon and Schoukens (2012)). From the FRF parametric models are identified for control design, flatness-based feed-forward, fault detection, etc.

In the case of electric drive trains the actuator used for the excitation is not a dedicated shaker but the driving electric motor of the plant belonging to the standard equipment. It is important to consider the constraints of the testbed and motor in terms of maximal stroke, velocity, acceleration and torque, while at the same time maximizing the output power of the actuator in favour of a high signal-to-noise ratio.

Different criteria for optimizing MFE signals have been defined, involving the amplitudes, phases or both:

- Minimization of the signal's crest factor, peak-to-peak value, maximization of the effective value, aiming at maximum actuator power and signal-to-noise ratio, e.g. Van der Ouderaa et al. (1988),
- Uniform coverage of the signal span (Mittelmann et al. (2007); Ong et al. (2011)),
- Matching of a given probability density function (PDF) of the signal amplitudes rather than just a uniform distribution (Myslinski et al. (2006)),
- Matching of a given power spectral density (PSD) and higher-order extensions (Pedro and Carvalho (2005)),
- Minimization of the parameter uncertainties of a parametric model or minimization of the maximum variance of the measured FRF (Schoukens et al. (1991)).

Optimizations are usually restricted to single signals, or possibly to input and output of a plant. Optimization results considering simultaneous constraints on position, velocity, acceleration and torque have not been reported yet, although these are natural requirements in the design of MFE signals for drive train identification applications.

It is the aim of this paper to develop an optimizer for MFE signals that maximizes the effective value for a given set of constraints on torque, acceleration, velocity and position as well as to verify the algorithm on a broad class of systems. The amplitudes and phases are calculated based on a priori knowledge available from system design. The effective value is optimized exclusively, because it is directly proportional to the power and signal-to-noise ratio (SNR) (Boyd (1986)). Optimizing one of the other criteria from above would lead to a reduction of the SNR compromising experimental time or signal quality. Also, more model-specific optimizations would require a relatively precise prior knowledge of the parameters (Pintelon and Schoukens (2012)) and even then the identification results are not always better than those of flat spectra (Lichota (2016)). A point of concern is also the time-efficient calculation because the resulting trajectory is plant-specific and accordingly it must be recalculated for each new plant.

2. RELATED WORKS

In the following some methods for numerically optimizing MFE signals with focus on their ability to integrate constraints into the optimization will be reviewed. These methods can be divided into two categories, firstly general purpose optimizers that could equivalently be used for other optimization problems and secondly those dedicated to the purpose of MFE optimization. The first category contains e.g. the exhaustive search (Ojarand et al. (2014)) and the optimization with genetic algorithms (Horner and Beauchamp (1996)). Constraints can usually be integrated using dedicated interfaces. Unfortunately, these algorithms are limited to small sets of frequencies due to excessive calculation times, while for the frequency-domain identification of multiple mass systems typically 100 to 1000 frequencies are needed.

Into the second category belongs the clipping algorithm, or time-frequency swapping algorithm (Van der Ouderaa et al. (1988)) as well as the sparing algorithm (Ojarand et al. (2014)). The consideration of constraints is not easily possible. A combination of a general-purpose algorithm and a dedicated crest factor optimizer is the iterative optimization of p-Norms based on Polya's algorithm/L_∞-algorithm as described by Guillaume et al. (1991). It can optimize system input and output simultaneously, also with constraints, because it is based on a trust region interior point method, a general-purpose optimizer, see e.g. Rivera et al. (2009); Lee et al. (2003). The problem of this simultaneous specification of magnitudes in frequency-domain and constraints in time domain is that it may lead to infeasible solutions.

In the next section two alternative possibilities of achieving the constrained effective value optimization are explained. One is based on the L_∞ optimization that allows an easy integration of constraints, the other is an extension of the clipping algorithm.

3. DESIGN OF MULTISINE EXCITATION SIGNALS

Two different approaches are presented for constrained MFE phase optimization after the common target has been formulated. They can equivalently be applied to translatory and rotary systems.

3.1 Optimization target

Starting with the MFE position signal in discrete-time:

$$q[n] = c_\mathrm{A} \sum_{k=1}^{N_k} A_k \cos\left(2\pi f_k T_\mathrm{s} n + \varphi_k\right), \tag{1}$$

the phases φ_k are to be optimized, along with the scaling factor c_A, while the relative amplitudes A_k and frequencies f_k are fixed. T_s is the sampling time, N_k is the number of frequency components. The spectrum design will be explained later. The optimization targets to find an optimal set of phases $\varphi_{k,\mathrm{opt}}$ that maximizes the effective value of the expected torque signal $\tau[n]$ while respecting constraints on position, velocity, acceleration and torque:

$$\varphi_{k,\mathrm{opt}} = \arg\max_{\varphi_k, c_\mathrm{A}} \left\{ \sqrt{\frac{1}{N_n} \sum_{n=1}^{N_n} \ddot{\tau}[n]^2} \right\}, \tag{2}$$

subject to

$$\begin{aligned} &|q[n]| \le |q|_\mathrm{max}, \quad |\dot{q}[n]| \le |\dot{q}|_\mathrm{max}, \\ &|\ddot{q}[n]| \le |\ddot{q}|_\mathrm{max}, \quad |\tau[n]| \le \tau_\mathrm{max} \quad \forall n \in [1, N_n]. \end{aligned}$$

3.2 L_∞ optimization

The first approach is explained for a single signal $q[n]$, firstly, later being extended to constraints on several signals. The main idea is that for the optimization (2) it is useful to minimize $\max\{|q[n]|\}$ (only considering the first constraint). For gradient-based minimization the cost function

$$L = \boldsymbol{e}^\mathrm{T} \boldsymbol{e}, \quad \boldsymbol{e} = (e_1, ..., e_n, ..., e_{N_n})^\mathrm{T} \tag{3}$$

with $e_n = q[n]^{p/2}$ is defined, in which $p = 2, 4, 8, ..., p_\mathrm{max}$ is increased in powers of two and for each step the optimization of the cost function is equivalent to minimizing the p-norm $||\boldsymbol{q}||_p$ with $\boldsymbol{q} = (q[1], q[2], ..., q[N_n])^\mathrm{T}$. Initially, c_A is set to 1. For p_max sufficiently large the p-norm converges to the Chebychev-norm $||\boldsymbol{q}||_\infty$, which is the maximum absolute value, but rather than optimizing $||\boldsymbol{q}||_\infty$ directly the cost function L is differentiable and less susceptible to local minima (Guillaume et al. (1991)).

In our implementation the gradient based optimizer is the trust region reflective algorithm for which the Jacobian matrix $\boldsymbol{J}$ is calculated analytically (Guillaume et al. (1991)):

$$J_{nk} = \frac{\partial e_n}{\partial \varphi_k} = -\frac{p}{2} q_n^{\frac{p}{2}-1} c_\mathrm{A} A_k \sin\left(2\pi f_k T_\mathrm{s} n + \varphi_k\right). \tag{4}$$

In order to expedite the calculation at the expense of increased memory consumption, $\boldsymbol{q}$ and $\boldsymbol{J}$ can be rewritten with an addition theorem [1]:

$$\begin{aligned} q[n] = c_\mathrm{A} \sum_{k=1}^{N_k} &[A_k \cos(2\pi f_k T_\mathrm{s} n) \cos(\varphi_k) \\ &- A_k \sin(2\pi f_k T_\mathrm{s} n) \sin(\varphi_k)], \\ \boldsymbol{q} = c_\mathrm{A} &\left(\boldsymbol{COS} \cdot \boldsymbol{L}_\mathrm{cos} - \boldsymbol{SIN} \cdot \boldsymbol{L}_\mathrm{sin}\right), \end{aligned} \tag{5}$$

with

$$\boldsymbol{L}_\mathrm{sin} = \begin{pmatrix} A_1 \sin(\varphi_1) \\ \vdots \\ A_{N_k} \sin(\varphi_{N_k}) \end{pmatrix}, \boldsymbol{L}_\mathrm{cos} = \begin{pmatrix} A_1 \cos(\varphi_1) \\ \vdots \\ A_{N_k} \cos(\varphi_{N_k}) \end{pmatrix} \tag{6}$$

and

$$\boldsymbol{SIN} = \begin{pmatrix} \sin(2\pi f_1 T_\mathrm{s} \cdot 1) & \cdots & \sin(2\pi f_{N_k} T_\mathrm{s} \cdot 1) \\ \sin(2\pi f_1 T_\mathrm{s} \cdot 2) & \cdots & \sin(2\pi f_{N_k} T_\mathrm{s} \cdot 2) \\ \vdots & \ddots & \vdots \\ \sin(2\pi f_1 T_\mathrm{s} \cdot N_n) & \cdots & \sin(2\pi f_{N_k} T_\mathrm{s} \cdot N_n) \end{pmatrix}, \tag{7}$$

$$\boldsymbol{COS} = \begin{pmatrix} \cos(2\pi f_1 T_\mathrm{s} \cdot 1) & \cdots & \cos(2\pi f_{N_k} T_\mathrm{s} \cdot 1) \\ \cos(2\pi f_1 T_\mathrm{s} \cdot 2) & \cdots & \cos(2\pi f_{N_k} T_\mathrm{s} \cdot 2) \\ \vdots & \ddots & \vdots \\ \cos(2\pi f_1 T_\mathrm{s} \cdot N_n) & \cdots & \cos(2\pi f_{N_k} T_\mathrm{s} \cdot N_n) \end{pmatrix}. \tag{8}$$

Similarly, J_{nk} can be rewritten:

[1] This has been inspired by the work of Ong et al. (2011).

$$J_{nk} = -\frac{p}{2} q_n^{\frac{p}{2}-1} c_\mathrm{A} A_k \left[\sin\left(2\pi f_k T_\mathrm{s} n\right)\cos(\varphi_k) + \cos\left(2\pi f_k T_\mathrm{s} n\right)\sin\left(\varphi_k\right)\right], \tag{9}$$

$$\boldsymbol{J} = -\boldsymbol{SIN} \odot \left[\frac{p}{2}\boldsymbol{q}^{\frac{p}{2}-1} \cdot \boldsymbol{L}_\mathrm{cos}^\mathrm{T}\right] - \boldsymbol{COS} \odot \left[\frac{p}{2}\boldsymbol{q}^{\frac{p}{2}-1} \cdot \boldsymbol{L}_\mathrm{sin}^\mathrm{T}\right]. \tag{10}$$

$\odot$ stands for the Hadamard product (entrywise product) and the exponentiation is meant entrywise. The expressions $\boldsymbol{COS}$ and $\boldsymbol{SIN}$ are calculated only once prior to the optimization of the first p-norm. Thus, during the optimization the effort for calculating $\boldsymbol{q}$ is reduced from $N_n \cdot N_k$ to $2 \cdot N_k$ sine or cosine evaluations. The same holds for $\boldsymbol{J}$.

To comply with the optimization target different signals and their constraints must be related. The underlying plant model for dimensioning is merely the overall inertia J_tot, which can be identified upfront with simple experiments. A more complex model would require prior knowledge that is usually not available before the identification. With $|\ddot{q}'|_\mathrm{max} = \min\left(|\ddot{q}|_\mathrm{max}, |\tau|_\mathrm{max}/J_\mathrm{tot}\right)$ the expression $\boldsymbol{q}$ is replaced by

$$\left(\frac{\ddot{\boldsymbol{q}}^\mathrm{T}}{|\ddot{q}'|_\mathrm{max}}, \frac{\dot{\boldsymbol{q}}^\mathrm{T}}{|\dot{q}|_\mathrm{max}}, \frac{\boldsymbol{q}^\mathrm{T}}{|q|_\mathrm{max}}\right)^\mathrm{T}. \tag{11}$$

The time derivatives are calculated from 1 after inserting t for $T_\mathrm{s} n$:

$$\dot{q}[n] = c_\mathrm{A} \sum_{k=1}^{N_k} 2\pi A_k f_k \cos\left(2\pi f_k T_\mathrm{s} n + \varphi_k + \pi/2\right), \tag{12}$$

$$\ddot{q}[n] = c_\mathrm{A} \sum_{k=1}^{N_k} 4\pi^2 A_k f_k^2 \cos\left(2\pi f_k T_\mathrm{s} n + \varphi_k + \pi\right). \tag{13}$$

In agreement with (11), $\boldsymbol{J}$ is also extended.

To prevent underflow or overflow, it is necessary to redefine the scaling factor c_A after each optimization in a certain norm. Here, it is set to the reciprocate value of the Chebychev norm $||\cdot||_\infty$ of (11). This also ensures that in the final signal the most restrictive constraint is just reached.

With this formulation relevant/active constraints are extracted natively, while loose constraints are ignored. The higher p, the more distinct is the dominance of the most restrictive constraint.

3.3 Modified clipping algorithm

In order to solve the same problem with the clipping algorithm a modification is necessary to optimize several signals (position, velocity, acceleration) simultaneously, as shown in Fig. 1, termed modified clipping algorithm (MCA).

In step 1 Newman phases are chosen as initial phases because they perform well for cosine based multisines (Boyd (1986)):

$$\varphi_k = \frac{\pi(k-1)^2}{N_k}. \tag{14}$$

c_A is set to 1. Steps 2 to 5 are necessary to allow for several signals to be optimized simultaneously. In step 2 the

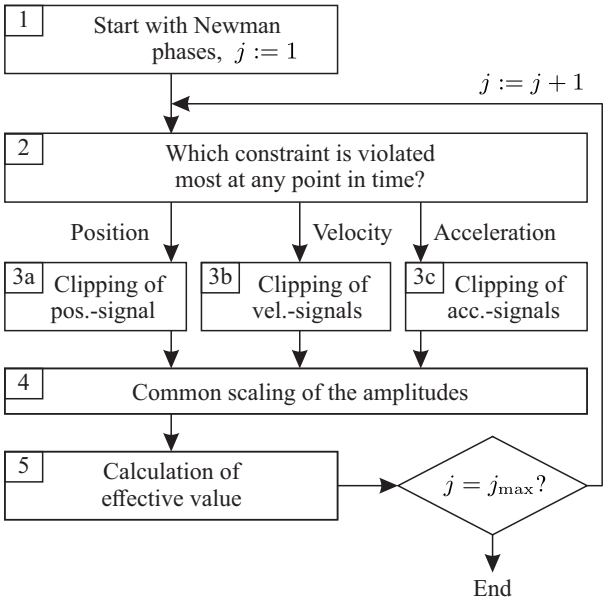

Fig. 1. Schematic of MCA

three signals are generated utilizing the addition theorem, e.g. the position signal according to equation (5). Then the signal $\boldsymbol{x}$ with the largest quantity $\max(|\boldsymbol{x}|)/|x|_\mathrm{max}$ is selected. $\boldsymbol{x}$ stands for $\boldsymbol{q}$, $\dot{\boldsymbol{q}}$ or $\ddot{\boldsymbol{q}}$, respectively and $|x|_\mathrm{max}$ stands for predefined constraints $|q|_\mathrm{max}$, $|\dot{q}|_\mathrm{max}$ or $|\ddot{q}|_\mathrm{max}$. Only this one signal is clipped by cutting off the peaks that exceed $CF \cdot \max(|\boldsymbol{x}|)$ with CF being the clipping factor. It is predefined somewhere in the range 0.5...1.0. [2] A Fourier series is calculated for the resulting signal,

$$X_k = \frac{1}{N_n} \sum_{n=<N_n>} \left(x[n] \cdot e^{-i\frac{2\pi}{N_n} n u}\right), \tag{15}$$

and the MFE phases φ_k are replaced by the phases of X_k, albeit with a shift depending on the signal type to revert the shifts in (1), (12), (13):

$$\varphi_k = \begin{cases} \angle X_k & \text{for position} \\ \angle X_k - \pi/2 & \text{for velocity} \\ \angle X_k - \pi & \text{for acceleration} \end{cases}. \tag{16}$$

In step 4 the scaling factor c_A is recalculated so that the most restrictive constraint is just reached. In the 5th step the effective value is calculated. If $N_k < N_n$, it is faster to calculate it in frequency-domain, rather than in time-domain (Van der Ouderaa et al. (1988)):

$$x_\mathrm{Eff} = c_\mathrm{A} \sqrt{\sum_{k=1}^{N_k} \frac{A_k^2}{2}}. \tag{17}$$

The phase vector with highest x_Eff ever achieved is stored as the result. This is necessary because the effective value is not generally monotonous. After k_max iterations the loop is terminated.

As a past processing step for both algorithms the MFE phases are shifted in order to reduce the transient of the following identification experiment by matching position, velocity and acceleration. While any position can be a valid initial position, the initial velocity and acceleration should be as small as possible. This is achieved by searching for

[2] Experiments with a per-sample-selection of the signal to clip showed inferior results in most cases.

all time instances with zero crossings in the velocity and then choosing the one with minimum acceleration.

3.4 Magnitude spectrum design

Although the magnitudes A_k could be designed arbitrarily, for the following investigations they are defined in agreement with the constraints as a function of the frequency. A constant torque spectrum over all frequencies would lead to low magnitudes at high frequencies given the constraints on position and velocity. Here the relative magnitudes are defined such that all constraints were just reached if each spectral line was applied on its own. Depending on the frequency at least one of the constraints is always active. Frequencies at which two constraints are active simultaneously are called corner frequencies. They will be used later to compare the algorithms for different relations of constraints. The position-velocity corner frequency it given by

$$|q|_{\max} = A_{k,\mathrm{C1}} \quad \text{and} \quad |\dot{q}|_{\max} = 2\pi f_{k,\mathrm{C1}} A_{k,\mathrm{C1}}$$
$$\Leftrightarrow f_{k,\mathrm{C1}} = \frac{|\dot{q}|_{\max}}{2\pi\,|q|_{\max}}. \tag{18}$$

Equivalently for velocity-acceleration:

$$f_{k,C2} = \frac{|\ddot{q}|_{\max}}{2\pi\,|\dot{q}|_{\max}}, \tag{19}$$

and position-acceleration:

$$f_{k,C3} = \sqrt{\frac{|\ddot{q}|_{\max}}{4\pi^2\,|q|_{\max}}}. \tag{20}$$

The behaviour of the optimizers is analysed with respect to these corner frequencies next.

4. RESULTS

In this section the performance of the two algorithms is compared with the ordinary clipping algorithm that considers only the input signal during the optimization, called standard clipping algorithm as a baseline. In Fig. 1 all the steps still apply, except that in step 2 only the acceleration signal is calculated and clipped in step 3a.

The optimized multisine signals are generated for

$$f_1, f_2, ..., f_{200} = 0.5\,\mathrm{Hz}, 1\,\mathrm{Hz}, ..., 100\,\mathrm{Hz} \tag{21}$$

with a sampling frequency of 1000 Hz, which is 10 times more than the highest payload frequency [3]. The clipping algorithms are run for 400 iterations with CF increasing linearly from 0.5 to 1.0, while the L_∞ optimization is performed for $p = 2, 4, ..., 512$ and at each step a maximum of 400 iterations of the gradient based optimizer are allowed, although often the solution is found earlier.

The three algorithms are compared for different corner frequencies in Fig. 2 to 4. The corner frequency effects the magnitude calculation according to section 3.4 as well as the optimization. Although it is possible that all three constraints (position, velocity and acceleration) each determine the amplitudes in a certain frequency range so

[3] In Guillaume et al. (1991) and Ong et al. (2011) two different formulas are given for the maximally expectable overshoot in terms of the ratio sampling frequency vs. max. payload frequency. It seems that 10 is a good compromise.

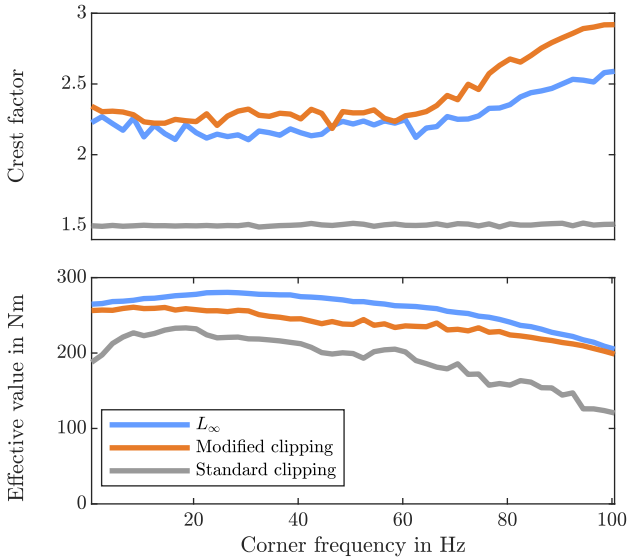

Fig. 2. Effective value and crest factor against corner frequency position-velocity

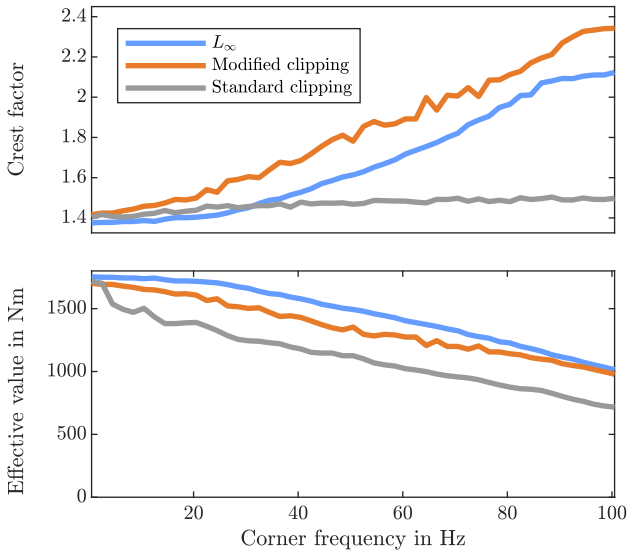

Fig. 3. Effective value and crest factor against corner frequency velocity-acceleration

that two corner frequencies lie in the valid frequency range (0.5 Hz...100 Hz), only the case of one corner frequency at a time is considered. The third constraint, not involved in the experiment is set to a high value which is never reached by the multisine signal.

The figures show the effective value against the frequency, which is the primary optimization target, but also the crest factor for comparison:

$$Cr = \frac{||\boldsymbol{q}||_\infty}{q_{\mathrm{Eff}}}. \tag{22}$$

As a result of the comparison it can be seen that the standard clipping creates signals with a lower effective value in almost all situations although the crest factor is constantly good (1.4...1.5). This is because it optimizes the acceleration signal exclusively, although depending on the corner frequency a different constraint may be more critical. In Fig. 3 and 4 the same effective value is reached

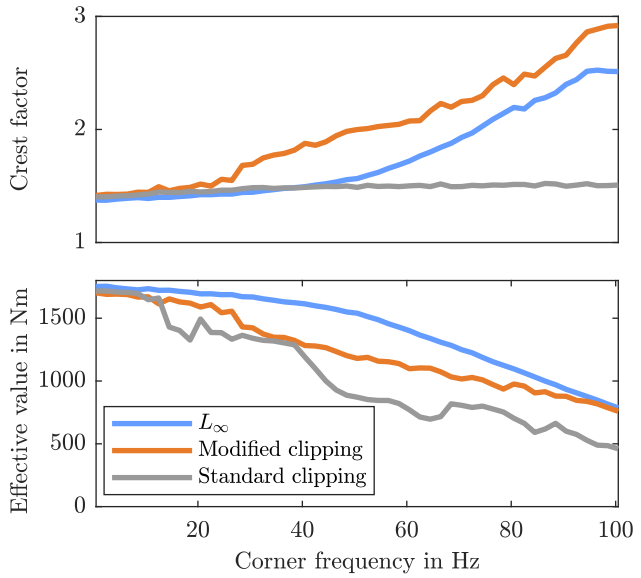

Fig. 4. Effective value and crest factor against corner frequency position-acceleration

at the lowest corner frequency as with the MCA. The reason is that at this point the velocity constraint has no effect and only the acceleration constraint is restrictive. In Fig. 2 the standard clipping is always inferior, because for no corner frequency the acceleration constraint is restrictive. The fact that in most situations a better effective value is achieved with the MCA than with the standard clipping shows the superiority of the MCA. In the multiple constraints case optimizing the crest factor of the input alone is questionable. Rather, the effective value should be optimized.

Regarding the performance of the L_∞ algorithm, it can be seen that it is always even better than the MCA, both in effective value and in crest factor. This can be explained by the generally better solutions achieved with L_∞ (Schoukens et al. (1991)). Also, the simultaneous optimization of several signals is readily possible in contrast to the MCA, where no per-sample-selection of the most critical signal is realized.

The approximate calculation times of our Matlab implementation have been captured on a 3.4 GHz Skylake CPU with one core in use and DDR4 Ram as follows, standard clipping: 3.4 s, MCA: 4.4 s, L_∞: 7:30 min. Although further performance improvements may be possible, it can be seen that L_∞ is distinctly slower than the other two and MCA tends to be a bit slower than standard clipping. So, although L_∞ performs slightly better in effective value, its considerably longer calculation time may be prohibitive in some applications, while the MCA is still competitive.

Fig. 5 deals with the path selection in Fig. 1, step 3 for the MCA. Depending on the corner frequency the signal with lower derivative order is selected in a certain percentage of the iterations, e.g. position, while in all other iterations the signal with the higher derivative order is selected and clipped, e.g. velocity. The figure shows for each of the three different corner frequencies how often the signal with lower derivative order is selected.

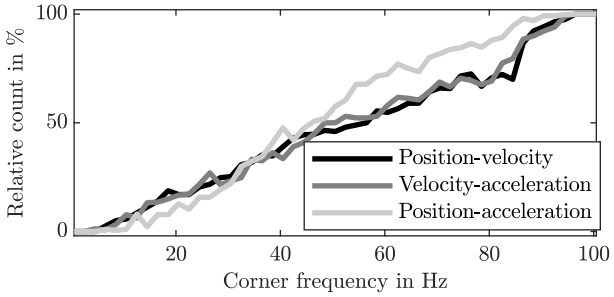

Fig. 5. Step 3 in Fig. 1: Number of iterations in which the signal of lower derivative is clipped, normalized to the overall number of iterations.

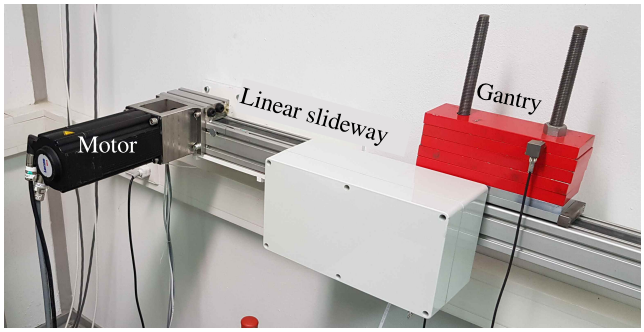

Fig. 6. Experimental testbed

It can be seen that at the margins $(0.5\,\text{Hz}, 100\,\text{Hz})$ this percentage is either 0 % or 100 %, meaning that a further extension of the considered corner frequencies would be pointless. Also, the amplitude spectrum would not change beyond these frequencies. Strictly speaking, this does not hold equally for the L_∞ optimization which always considers all three signals, but because of the high exponentiation signals with lower amplitudes have a minor effect, too.

5. EXPERIMENTAL VALIDATION

A linear belt drive, see Fig. 6, with the following properties serves as a validation testbed: maximum targeted motor torque 1 Nm and linear velocity 0.05 m/s, belt pulley radius: 0.0159 m, direct drive. The equivalent moment of inertia of motor and linear gantry has been identified to be $0.00516\,\text{kgm}^2$. According to (19) the velocity-acceleration corner frequency can be calculated for this testbed:

$$|\dot{q}|_{\max} = \frac{0.05\,\text{m/s}}{0.0159\,\text{m}} \quad \text{and} \quad |\ddot{q}|_{\max} = \frac{1\,\text{Nm}}{0.00516\,\text{kgm}^2}$$
$$\Rightarrow f_{k,\text{C1}} = \frac{|\ddot{q}|_{\max}}{2\pi\,|\dot{q}|_{\max}} = 9.81\,\text{Hz}. \tag{23}$$

The other two corner frequencies are irrelevant, because the position stroke is large. In three separate experiments the different excitation signals from the above methods are applied to the testbed, each with a duration of 22 s and a frequency range of 0.5 Hz, 1 Hz, ..., 100 Hz. 22 s is the minimum duration that allows to extract 11 periods of the base frequency later. The following effective values are achieved, standard clipping: 0.632 Nm, MCA: 0.692 Nm, L_∞: 0.723 Nm. Cascaded torque, velocity and position

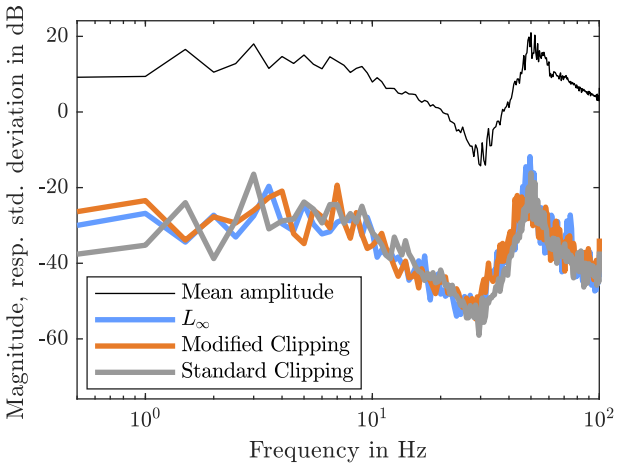

Fig. 7. Standard deviations $\sigma(j\omega)$ of the FRF estimates from three excitation signals and the amplitude of the mean FRF from the measurement with the standard clipping signal

control is used for the closed-loop identification with reference position, velocity and torque defined by the MFE signal.

From $M+1$ consecutive periods of the torque-velocity measurement mean and standard deviation of the FRF are calculated (Schoukens et al. (2009)):

$$\hat{G}_{uy} = \frac{\hat{Y}}{\hat{U}} = \frac{\frac{1}{M}\sum_{m=2}^{M+1} Y^{[m]}}{\frac{1}{M}\sum_{m=2}^{M+1} U^{[m]}}, \tag{24}$$

$$\hat{\sigma}^2_G \approx \frac{|\hat{G}|}{\sqrt{M}} \cdot \sqrt{\frac{\hat{\sigma}^2_y}{|\hat{Y}|^2} + \frac{\hat{\sigma}^2_u}{|\hat{U}|^2} - 2\mathrm{Re}\left(\frac{\hat{\sigma}^2_{uy}}{\hat{Y}\hat{U}}\right)}. \tag{25}$$

Index k indicating frequency dependencies has been neglected for notational simplicity. $U^{[m]}$ and $Y^{[m]}$ are the DFT spectra of the m-th period of the torque, resp. velocity signal. The first period (2 s) is discarded to allow for settling, $M = 10$. $\hat{\sigma}^2_u$ and $\hat{\sigma}^2_y$ are the empirical variances, $\hat{\sigma}^2_{uy}$ is the empirical covariance of torque and velocity:

$$\hat{\sigma}^2_u = \frac{1}{M-1}\sum_{m=2}^{M+1}\left|U^{[m]} - \hat{U}\right|^2, \tag{26}$$

equally for Y, and

$$\hat{\sigma}^2_{uy} = \frac{1}{M-1}\sum_{m=2}^{M+1}\left[\left(Y^{[m]} - \hat{Y}\right)\overline{\left(U^{[m]} - \hat{U}\right)}\right]^2. \tag{27}$$

The amplitude of $\hat{G}_{uy}$ and the standard deviation $\hat{\sigma}^2_{uy}$ for each method are shown in Fig. 7. Apparently, the one-mass model with parameter J_{tot} was not an accurate model, as can be seen from the antiresonance-resonance behaviour and the zero slope at low velocities.

From Fig. 7 a clear difference in the noise level obtained from the three methods cannot be seen. Experiments with higher torque and velocity ratings at the same testbed (10 Nm) showed a higher, not lower standard deviation. This indicates non-repeatability in the system, which affects the measurement more than the sensor noise or stated differently the sensors are of very high quality.

To investigate the effect of increased sensor noise due to lower sensor quality, longer cables, imperfect shielding and

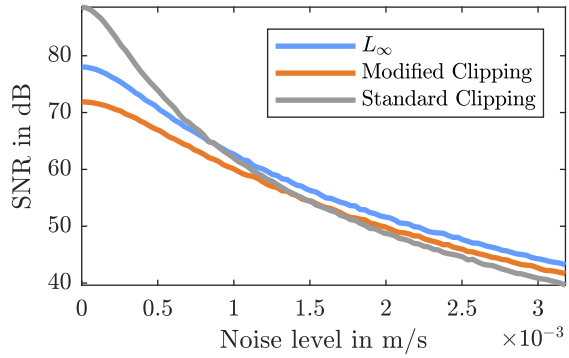

Fig. 8. Signal to noise ratio of the velocity measurement for different levels of additive white sensor noise

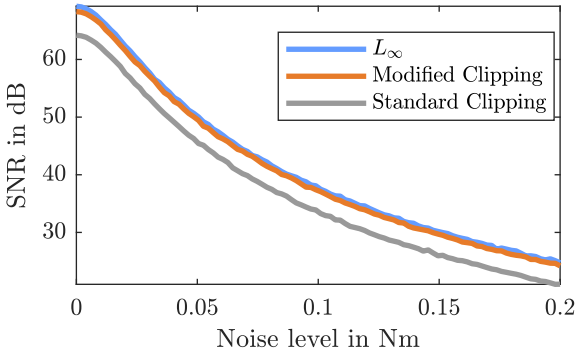

Fig. 9. Signal to noise ratio of the torque measurement for different levels of additive white sensor noise

so on the SNR ratios of the measured torque and velocity are determined for different levels of subsequently additive, random Gaussian sensor noise: From the 10 measurements the standard deviation is calculated separately for each time step and then averaged over all time samples. This calculation is done for the original measurements as well as for the measurement signals with added noise of increasing power, see Fig. 8, 9.

In Fig. 8 the SNRs at 0 added Gaussian noise show a relation of the three methods that is not expected from the effective values of the excitation signals. As a possible explanation, the SNR is high and the sensor noise contributes only marginally to inter-measurement variations, while other, non-reproducible effects overwhelm. However, with increased additive noise the relations of SNRs for the three methods converge to the pattern of L_∞ being best, followed shortly by MCA and finally standard clipping.

For the torque measurement in Fig. 9 a similar effect as in Fig. 8 can be observed, except that the initial relation of the SNRs already corresponds to the effective values. Repeating this experiment at different excitation amplitudes has shown that the initial SNR is highly unrepeatable for torque and velocity while always the same pattern at high noise levels is found. This tendency cannot be seen so clearly in the standard deviation of the FRFs for additive noise, equation (25), not shown here.

6. DISCUSSION

The proposed concept of system-specific corner freqencies allows an efficient optimization and a transfer of the results to other testbeds. It must, however, be admitted

that in many cases the corner frequencies are below the lowest excitation frequency so that the simultaneous consideration of different constraints leads to the same results as with the standard clipping. This is expectable if the position stroke is very long and the maximal velocity is high. In this case considering the additional constraints will raise the calculation time, while having no other effect, except that the trajectory can be driven with more confidence.

It was shown in experiments that the SNR is clearly dependent on the effective value of the excitation only if the sensor noise is high and thus dominates the SNR. This result was obtained only by adding random noise to the measurement; the original measurements did not show a clear quality dependency on the effective value. It seems that the quest for optimized crest factor or effective value is of minor practical importance, at least if the sensors are good, as previously observed by Sanchez et al. (2011). The direct-drive testbed under study is equipped with a motor with 13.7 Nm torque rating, but even at 1 Nm maximum torque the FRF can be measured well. It is to be expected that for other setups with gear and high friction a high effective value of the excitation could be more important.

7. CONCLUSION

In this work the problem of multisine optimization subject to diverse constraints was considered and applied to excitation of electric drive trains. At the outset the state of the art was reviewed with the result that the clipping algorithm has only been applied to single signals, while the L_∞ algorithm allows to incorporate such constraints naturally.

A promising realization of the clipping algorithm was proposed in this work for the integration of constraints, called MCA, and compared with the L_∞ algorithm, which is formulated in a way that it considers the same constraints. For the comparison crest factors and effective values were reported in terms of corner frequencies that describe a given set of constraints in a unified way.

It was found that the effective value should be the criterion to optimize in multiple constraint situations, not the crest factor of the input signal, as customary in industry. This difference is most important if the maximum velocity or the maximum stroke of movement are small. The L_∞ showed a slightly better effective value than the MCA throughout. In regard to calculation time the MCA is approximately a hundred times faster than the L_∞ algorithm.

Experiments on an industry-like testbed were performed to investigate the practical relevance of the comparison. Here, a significant reduction in the signal-to-noise ratio of the identified frequency response function could not be exposed, but the results indicate that setups with lower sensor quality would very well benefit from high effective values.

ACKNOWLEDGEMENTS

This work was sponsored by the AiF (Arbeitsgemeinschaft industrieller Forschungsvereinigungen Otto von Guericke e.V.) and managed by the FVA (Forschungsvereinigung Antriebstechnik e.V.) both in Germany.

REFERENCES

Boyd, S. (1986). Multitone signals with low crest factor. *IEEE circuits and systems*, 33(10), 1018–1022.

Guillaume, P., Schoukens, J., Pintelon, R., and Kollar, I. (1991). Crest-factor minimization using nonlinear Chebyshev approximation methods. *IEEE Transactions on Instrumentation and Measurement*, 40(6), 982–989.

Horner, A. and Beauchamp, J. (1996). A genetic algorithm-based method for synthesis of low peak amplitude signals. *The Journal of the Acoustical Society of America*, 99(1), 433–443.

Lee, H., Rivera, D.E., and Mittelmann, H.D. (2003). Constrained minimum crest factor multisine signals for" plant-friendly" identification of highly interactive systems. *IFAC Proceedings Volumes*, 36(16), 915–920.

Lichota, P. (2016). Inclusion of the D-optimality in multisine manoeuvre design for aircraft parameter estimation. *Journal of Theoretical and Applied Mechanics*, 54(1), 87–98.

Mittelmann, H.D., Pendse, G., Rivera, D.E., and Lee, H. (2007). Optimization-based design of plant-friendly multisine signals using geometric discrepancy criteria. *Computational Optimization and Appl.*, 38(1), 173–190.

Myslinski, M., Remley, K.A., McKinley, M.D., Schreurs, D., and Nauwelaers, B. (2006). A measurement-based multisine design procedure. In *2006 International Workshop on Integrated Nonlinear Microwave and Millimeter-Wave Circuits*, 52–55. IEEE.

Ojarand, J., Min, M., and Annus, P. (2014). Crest factor optimization of the multisine waveform for bioimpedance spectroscopy. *Phys. Meas.*, 35(6), 1019.

Ong, M.S., Kuang, Y.C., Liam, P.S., and Ooi, M.P.L. (2011). Multisine with optimal phase-plane uniformity for adc testing. *IEEE Transactions on Instrumentation and Measurement*, 61(3), 566–578.

Pedro, J.C. and Carvalho, N.B. (2005). Designing multisine excitations for nonlinear model testing. *IEEE Microwave Theory and Techniques*, 53(1), 45–54.

Pintelon, R. and Schoukens, J. (2012). *System identification: a frequency domain approach*. John Wiley & Sons, Inc., Hoboken, New Jersey.

Rivera, D.E., Lee, H., Mittelmann, H.D., and Braun, M.W. (2009). Constrained multisine input signals for plant-friendly identification of chemical process systems. *Journal of Process Control*, 19(4), 623–635.

Sanchez, B., Vandersteen, G., Bragos, R., and Schoukens, J. (2011). Optimal multisine excitation design for broadband electrical impedance spectroscopy. *Measurement Science and Technology*, 22(11), 115601.

Schoukens, J., Guillaume, P., and Pintelon, R. (1991). Design of multisine excitations. In *International Conference on Control 1991. Control'91*, 638–643. IET.

Schoukens, J., Vandersteen, G., Barbé, K., and Pintelon, R. (2009). Nonparametric preprocessing in system identification: a powerful tool. In *European Control Conference (ECC)*, 1–14. IEEE.

Van der Ouderaa, E., Schoukens, J., and Renneboog, J. (1988). Peak factor minimization using a time-frequency domain swapping algorithm. *IEEE Transactions on Instrumentation and Measurement*, 37(1), 145–147.